Assessment of Detailed Photoreceptor Structure and Retinal Sensitivity in Diabetic Macular Ischemia Using Adaptive Optics-OCT and Microperimetry

Felix Datlinger,[1] Lorenz Wassermann,[1] Adrian Reumueller,[1] Dorottya Hajdu,[1] Irene Steiner,[3] Matthias Salas,[2] Wolfgang Drexler,[2] Michael Pircher,[2] Ursula Schmidt-Erfurth,[1] and Andreas Pollreisz[1]

[1]Department of Ophthalmology and Optometry, Medical University of Vienna, Vienna, Austria
[2]Center of Medical Physics and Biomedical Engineering, Medical University of Vienna, Vienna, Austria
[3]Center of Medical Statistics, Informatics and Intelligent Systems, Medical University of Vienna, Vienna, Austria

Correspondence: Andreas Pollreisz, Department of Ophthalmology and Optometry, Medical University Vienna, Waehringer Guertel 18-20, 1090 Vienna, Austria; andreas.pollreisz@meduniwien.ac.at.

Received: March 8, 2021
Accepted: August 14, 2021
Published: October 4, 2021

Citation: Datlinger F, Wassermann L, Reumueller A, et al. Assessment of detailed photoreceptor structure and retinal sensitivity in diabetic macular ischemia using adaptive optics-OCT and microperimetry. *Invest Ophthalmol Vis Sci.* 2021;62(13):1. https://doi.org/10.1167/iovs.62.13.1

Purpose. The purpose of this study was to assess density and morphology of cone photoreceptors (PRs) and corresponding retinal sensitivity in ischemic compared to nonischemic retinal capillary areas of diabetic eyes using adaptive optics optical coherence tomography (AO-OCT) and microperimetry (MP).

Methods. In this cross-sectional, observational study five eyes of four patients (2 eyes with proliferative diabetic retinopathy (DR) and 3 eyes moderate nonproliferative DR) were included. PR morphology and density was manually assessed in AO-OCT en face images both at the axial position of the inner-segment outer segment (IS/OS) and cone outer segment tips (COSTs). Retinal sensitivity was determined by fundus-controlled microperimetry in corresponding areas (MP-3, Nidek).

Results. In AO-OCT, areas affected by capillary nonperfusion showed severe alterations of cone PR morphology at IS/OS and COST compared to areas with intact capillary perfusion (84% and 87% vs. 9% and 8% of area affected for IS/OS and COST, respectively). Mean reduction of PR signal density in affected areas compared to those with intact superficial capillary plexus (SCP) and deep capillary plexus (DCP) perfusion of similar eccentricity was –38% at the level of IS/OS ($P = 0.01$) and –39% at the level of COST ($P = 0.01$). Mean retinal sensitivity was 10.8 ± 5.4 in areas affected by DCP nonperfusion and 28.2 ± 1.5 outside these areas ($P < 0.001$).

Conclusions. Cone PR morphology and signal density are severely altered in areas of capillary nonperfusion. These structural changes are accompanied by a severe reduction of retinal sensitivity, indicating the importance of preventing impaired capillary circulation in patients with DR.

Keywords: adaptive optics optical coherence tomography (AO-OCT), microperimetry (MP), diabetic macular ischemia (DMI), photoreceptors (PRs)

Diabetic retinopathy (DR) is characterized by pericyte loss around retinal capillaries and small arterioles, thickening of the basement membrane, fibrosis of the retinal vessel wall, and endothelial cell death.[1,2] These vascular alterations lead to capillary closure, the hallmark of diabetic macular ischemia (DMI), which is clinically characterized by an increased size of the foveal avascular zone and the presence of capillary nonperfusion in the macular region.[2–4] DMI is associated with progression of DR, irreversible visual loss, and reduced visual acuity gain even after treatment with intravitreal anti-VEGF agents.[3,5–11] Fluorescein angiography has been the gold standard in diagnosing and quantifying DMI.[3,12] However, fluorescein angiography does not allow for the evaluation of individual capillary plexus with the deep capillary plexus (DCP) particularly inaccessible due to the overlaying fluorescence from the superficial capillary plexus (SCP). However, optical coherence tomography angiography (OCTA) permits a depth-resolved differentiation and visualization of different retinal vascular layers noninvasively within seconds.[13] There is evidence from clinical trials that capillary nonperfusion at the level of the DCP, as determined with OCTA, colocalizes with alterations of the outer retina and in particular changes in the photoreceptor (PR) layer as assessed with OCT.[14,15] Because the introduction of fundus-guided microperimetry (MP) functional testing of PR in specific retinal locations is feasible.[16,17] Only limited data are available on the relationship between PR layer integrity and retinal function in areas affected by DMI.[15] Recently, adaptive optics (AOs) assisted imaging has enabled in vivo evaluation of individual PR cells by measuring and correcting for wavefront aberrations of the eye in real-time.[18–21] The combination of AO and OCT

Investigative Ophthalmology & Visual Science

(AO-OCT) enables a volumetric three-dimensional assessment of the outer retina allowing for a separate evaluation of the PR inner segment/outer segment junction (IS/OS) and the cone outer segment tips (COSTs).[22,23] In this pilot study, we combined AO-OCT, OCTA, and spectral domain (SD)-OCT with MP measurements to assess the relationship between retinal capillary perfusion, three-dimensional PR integrity at the level of individual PR cells and retinal sensitivity in patients with DMI.

Methods

In this prospective study, patients were recruited from the outpatient clinic for DR at the Department of Ophthalmology at the Medical University of Vienna. The study was approved by the institutional review board of the Medical University of Vienna, adhered to the tenets of the Declaration of Helsinki, and was conducted according to the Guidelines for Good Clinical Practice.

Patients

Inclusion criteria were eyes from patients with diabetes (diabetes mellitus type 1 or 2) with moderate nonproliferative to proliferative DR and the presence of at least one area of DCP nonperfusion, as assessed with OCTA. Any region of interest (either inside the area of DCP nonperfusion, in the border region between intact DCP perfusion and DCP nonperfusion, or in areas with intact SCP and DCP perfusion without directly adjacent DCP nonperfusion, had to be free from fluid, pre- or intra-retinal material, or hemorrhages.

To allow for valid intra-individual comparison of PR signal density values, AO-OCT images of at least one ischemic and one corresponding area with intact capillary perfusion with a difference of equal or less than 1 degree of foveal eccentricity had to be available of the same patient. Thus, we could ensure that intra-individual comparison of PR density values, which are known to decrease with increasing distance from the foveal center, were not influenced by a varying extent of foveal eccentricity.[24,25]

Minimal pupillary diameter was required to be at least 5 mm with a regular pupil contour after instillation of 1.0% tropicamide (Mydriaticum Agepha, Vienna, Austria) and 2.5% phenylephrine hydrochloride. The spherical equivalent had to be below +/- 5 diopters and cylindrical astigmatism below 2 diopters. General exclusion criteria were the presence of any retinal disease (e.g. epiretinal membranes, age-related macular degeneration, macular holes, uveitis, etc.) other than DR in the study eye. Cataract with more severe stages than nuclear opacification 3, nuclear color 3, cortical cataract 2, and posterior subcapsular cataract 0.5 according to the Lens Opacification Classification System III,[26] or corneal scarring excluded patients from study participation. Further, no intraocular surgery except uncomplicated cataract surgery with a mono-focal capsular bag supported acrylic lens without development of posterior capsule opacification or anterior capsule contraction syndrome was allowed prior to study inclusion.

Visual Acuity Testing and Standard OCT/OCTA Imaging

Visual acuity testing (ARK-1s; Nidek Co. Ltd., Gamagori, Japan) and biometry including axial length and keratometry (IOL Master 500; Carl Zeiss Meditec, Jena, Germany) were performed before medical mydriasis. The presence of ischemia of the SCP and DCP was evaluated using 20 degrees × 20 degrees swept source OCTA scan, which corresponds to a field of view of approximately 6 mm × 6 mm, centered on the fovea (Plex Elite; Carl Zeiss Meditec, Germany). SD-OCT (Spectralis HRA2 + OCT; Heidelberg Engineering, Heidelberg, Germany) was performed using the following settings: 20 degrees × 20 degrees, high resolution mode, and automated real-time tracking with 15 to 20 averaged scans. OCT and OCTA images were studied meticulously to exclude the presence of pre- or intra-retinal material, such as hard exudates, spot bleedings, or intraretinal cysts before selecting the areas of interest, where AO-OCT and MP was performed. MP (MP-3; Nidek Co. Ltd., Gamagori, Japan) was performed in the study eye, using either the maculopathy or drusen/pigment epithelium detachment grid provided by the system's software that was centered on the fovea. In one patient (patient no. 2), the grid was positioned slightly temporal from the foveal center because the ischemic area of interest was outside the grid, when centered on the fovea. If necessary, individual MP spots were added inside the areas affected by DCP nonperfusion, in the perfused border region just outside the ischemic area and inside perfused areas with similar eccentricity to the fovea.

Adaptive Optics OCT Imaging

AO-OCT imaging was performed with a system developed at the Center for Medical Physics and Biomedical Engineering at the Medical University of Vienna which had been clinically applied before.[23,25,27–29] In brief, the system combines an AO fundus camera and AO-OCT in a compact system by utilizing a deformable mirror (Mirao52-e RC; Imagine Eyes, Orsay, France) and a Shack Hartmann wavefront sensor (Haso First; Imagine Optics, Orsay, France) for AO enhancement.[30,31] The OCT system is operated at 840 nm with an A-scan rate of 200 kHz and an axial resolution in the retina of approximately 5 µm. Each AO-OCT volume consists of 400 B-scans and covers a field of view of 2 degrees × 2 degrees. Acquisition time of one AO-OCT volume is less than 1 second. A live stream of the B-scan allows for optimization of the image quality by manually adjusting the focus onto the different photoreceptor layers. To localize the regions of interest, retinal vessels from the OCTA images were used as landmarks on the AO fundus camera live-image of the system. When a region of interest was localized on the AO fundus camera live image, several AO-OCT volumes of this region were acquired.

AO-OCT Image Analysis

First, axial motion artifacts caused by involuntary head movements of the patients were removed by axially aligning single AO-OCT B-scans next to each other using a cross correlation method in Matlab 2017b (MathWorks, Inc., Natick, MA, USA).[30,31] En face images were extracted from the registered AO-OCT at the axial position of IS/OS as well as COST using the Z-Project function. Two to six consecutive slices in the z-axis, each with a size of one pixel, were used to create the AO-OCT en face images of PR IS/OS and COST.

Within the same region of interest, the number of PR signals was counted manually in the en face IS/OS and COST images in up to 2 areas with intact SCP and DCP perfusion and 2 areas with DCP nonperfusion, each measuring 80 ×

Investigative Ophthalmology & Visual Science

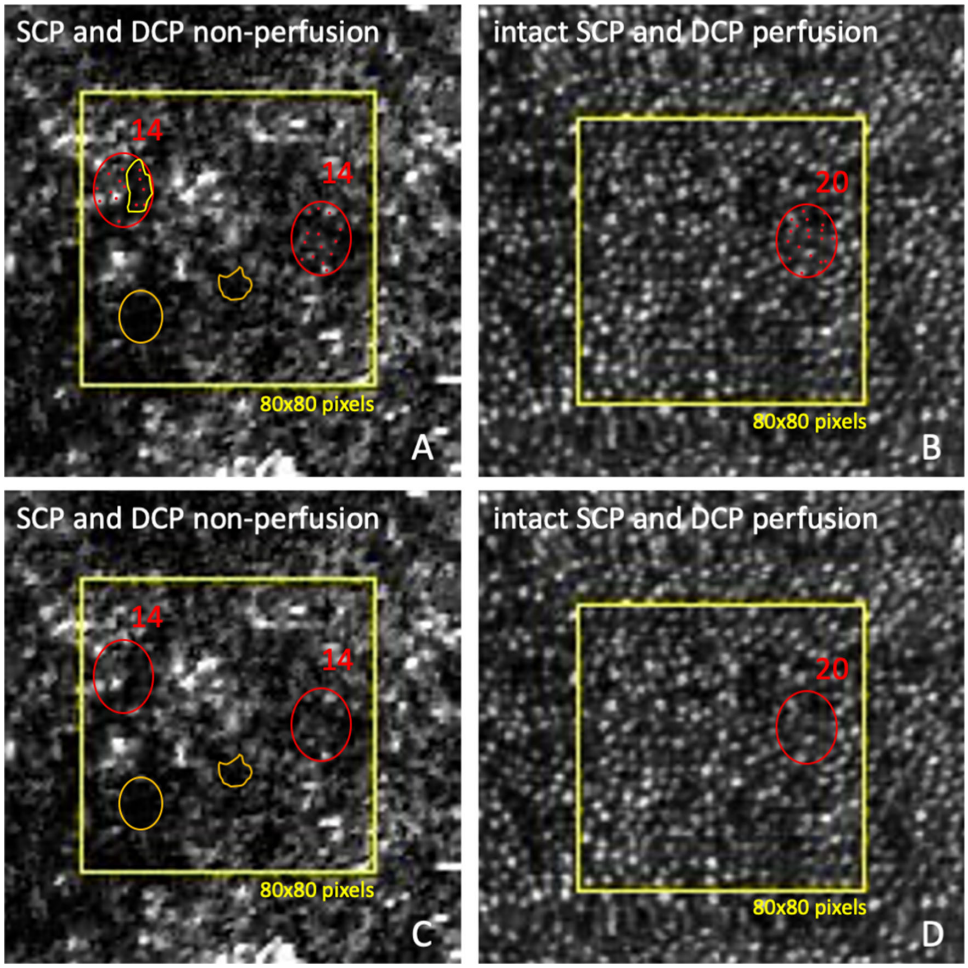

Figure 1. Example of manual counting of photoreceptor (PR) signals on en face AO-OCT images of a 58-year-old male patient with diabetes type II and moderate DR (patient 1). PR signals were manually counted in areas of 80 × 80 pixels (**A, B**; *yellow box*). Severe distortion and patchy loss of PR signals is seen in the area affected by SCP and DCP nonperfusion **A**. In contrast, PRs are densely packed and regularly arranged in an area of similar foveal eccentricity in the same eye where SCP and DCP perfusion was intact **B**. Weak PR signals are predominantly seen in the area affected by SCP and DCP nonperfusion **A**. These weak signals were also considered for PR density calculations **A** (*red dots encircled in yellow*). Very weak signals, clearly below the size of any PR signal found in areas with intact perfusion **A** (*encircled in orange*) were not considered for counting, since they either represent noise that derives from the underlying retinal pigment epithelium or severely damaged PRs. The representatively selected areas *encircled in red* serve to further illustrate PR signal counting **A** and **B**. Each *small red dot* inside the *red circles* represents one PR signal. The total number of PR signals inside each representatively counted area is written above the respective circle. The lower column (**C, D**) shows the same information as the upper column **A** and **B** without the *red dots* inside the *red circles* for better visibility of PR signals in these areas.

80 pixels, which corresponds to a size of approximately 150 × 150 µm in an eye with 23.5 mm axial length. Figure 1 shows an example of the PR signal counting and different PR signal strengths. PR signal density at the level of IS/OS and COST per mm^2 was then calculated by considering the axial eye length of each patient.

PR morphology was assessed both at the axial position of IS/OS as well as COST according to a grading scheme previously demonstrated by our group.[23] In brief, regular arrangement of PR morphology was present when densely packed, bright white round dots representing PRs could be observed, whereas irregular morphology was defined as attenuation or loss of these PR signals. We then measured the percentage of the area with PR irregularities. PR morphology was defined as unremarkable if an area showed PR abnormalities in less than 10% of the total area, mild, moderate, and severe if 10% to 33.33%, 33.34% to 66.66%, and more than 66.67% were affected, respectively. The morphological grading of PRs was assessed by two masked graders experienced in AO-OCT image analysis (authors F.D. and L.W.).

Normal distribution of PR signal density values was assessed using the Shapiro-Wilk test. With a *P* value of 0.40 (IS/OS) and 0.43 (COST), respectively, the data can be considered as approximately normally distributed. Therefore, a paired *t*-test, using one mean value per patient was used for statistical comparison of differences in PR signal density in areas affected by SCP and DCP nonperfusion and areas with intact capillary perfusion at the level of SCP and DCP of similar eccentricity within the same eye. For the statistical analysis of differences in retinal sensitivity between areas with and without DCP nonperfusion a mixed model with retinal sensitivity as dependent variable was calculated. Patients were taken as a random factor to consider for repeated measurements. The independent variable was the perfusion status of each area

Investigative Ophthalmology & Visual Science

(perfused/ischemic). The degrees of freedom were calculated using the Kenward-Roger approximation. One patient had measurements on both eyes. For this patient, only one eye was included.

Results

Patients' Demographics

Patient 1 was a 58-year-old with type II diabetes mellitus, patient 2 was a 34-year-old with type I diabetes mellitus, patient 3 was a 38-year-old with type I diabetes mellitus, and patient 4 was a 60-year-old with type II diabetes mellitus at the time of image acquisition. Recent HbA1c values of these patients ranged from 7.1% to 7.6%. No other systemic diseases were known in the two patients with diabetes mellitus type I. Well controlled hypertension was present in the other two patients with type II diabetes mellitus. Ophthalmic examination revealed moderate DR in the right eye of patient 1 (Fig. 2), moderate DR in the left and right eyes of patient 2 (Fig. 3), quiescent proliferative DR in the right eye of patient 3 (Supplementary Fig. S1), and proliferative DR in the right eye of patient 4 (Supplementary Fig. S2). Best-corrected visual acuity was 20/32 in patient 1, 25/20 in patient 2, 20/20 in patient 3, and 20/40 in patient 4. Patient 1 received 9 intravitreal anti-VEGF within 18 months prior to study inclusion and patient 4 received the last of 5 injections 22 months prior to the study visit, both due to diabetic macular edema. OCT scans routinely acquired at the patient's visits at the outpatient clinic showed that the edema never extended into any of the areas imaged with AO-OCT. Patient 2 did not receive any ocular treatment in either eye prior to study inclusion. Patient 3 had pan-retinal photocoagulation 2 years prior to the inclusion in this study due to active proliferative DR. For a summary of the patients' demographic characteristics, see Table 1.

Quantitative Evaluation of PR Signals at the Level of IS/OS and COST

PR signals were manually counted in 5 eyes of 4 patients with diabetes: 13 areas with nonperfused DCP, among them 3 areas where SCP perfusion was intact, and 23 areas with intact SCP and DCP perfusion. A maximum of two areas with intact DCP perfusion and DCP nonperfusion was counted per region of interest. In all 13 areas located within the 8 regions of interest affected by DCP nonperfusion, AO-OCT en face images showed a reduction in PR signal density both at the axial position of IS/OS and COST, when compared with areas of similar foveal eccentricity with intact SCP and DCP perfusion in the same eye (Table 2). Mean foveal eccentricity of all regions of interest with DCP nonperfusion and with intact SCP and DCP perfusion was 5.10 degrees (±2.2) and 5.11 degrees (±2) respectively.

Mean PR signal density in areas affected by DCP nonperfusion was 5653 ± 2105/mm^2 at IS/OS and 5654 ± 2252/mm^2 at COST compared to 9359 ± 3380/mm^2 at IS/OS and 9089 ± 3504/mm^2 at COST in areas with intact SCP and DCP perfusion of similar foveal eccentricity. The mean reduction of PR signal density in areas affected by DCP nonperfusion compared with areas with intact SCP and DCP perfusion of similar foveal eccentricity was –38% at IS/OS and –39% at COST (both $P = 0.01$). Table 2 lists mean PR signal density values for each region of interest and the corresponding perfusion status.

Qualitative Evaluation of PR Signal Morphology at the Level of IS/OS and COST

PR morphology was severely altered in all eight ischemic regions of interest both at IS/OS and COST. In contrast, PR morphology in the 13 areas with intact capillary perfusion was unaffected in 9 and 10 areas and mildly affected in 4 and 3 areas at IS/OS and COST, respectively. No area showed moderate morphological alterations.

The mean percentage of area affected by either attenuation or loss of PR signals was 84% and 87% for IS/OS and COST in the ischemic areas and 9% and 8% for IS/OS and COST in the areas with intact capillary perfusion. We found that agreement between the two graders was very good. Mean difference between grader 1 and 2 was 5.3% (±4.8) for IS/OS and 5.2% (±5.0%) for COST. Discrepancies between the 2 graders were present in only 3 out of 42 gradings (21 × IS/OS and 21 × COST). The 3 discrepancies were found in 2 regions of interest with intact capillary perfusion, where one grader assessed PR morphology as unaffected and the other as mildly affected with a mean difference of 10.8% between these gradings.

Correlation of PR Signal and Retinal Sensitivity Values

In AO-OCT en face images of PR signals at the level of IS/OS and COST were attenuated or completely lost in areas with DCP nonperfusion (see Figs. 2G, 2H, right from the white dotted line see Figs. 3D, 3E, lower half) and regularly arranged in areas with intact SCP and DCP perfusion either directly adjacent to areas affected by DCP non-perfusion (see Figs. 2G, 2H, left half see Figs. 3D, 3E, upper half) or in areas of similar foveal eccentricity without adjacent DCP nonperfusion (see Figs. 2J, 2K and Figs. 3G, 3H). Analogously to the AO-OCT enface images, AO-OCT B-scans also revealed hypo-reflectivity or loss of PR signals at IS/OS and COST in areas with DCP nonperfusion (see Fig. 2, F2, F4, I2, I4, right half, see Fig. 3, F2 left third, F4). Regular IS/OS and COST arrangement were seen in areas with intact SCP and DCP perfusion (see Fig. 2, L2, L4, see Fig. 3, I2, I4).

In areas with DCP nonperfusion, where AO-OCT revealed PR distortion and a reduction in PR signal density, retinal sensitivity was severely reduced in patient 1 (7 dB) and patient 3 (4 dB) and completely lost in patient 4 (0 dB; see Fig. 2C, Supplementary Fig. S1C, red boxes, Supplementary Fig. S2C, yellow box). Patient 2 presented with the smallest area of DCP nonperfusion measuring 330 µm × 290 µm (see Figs. 3A–C, yellow boxes). MP was unaffected (27 and 30 dB) in and around this area (see Fig. 3C, yellow box). A reduction in PR signal density both at level of IS/OS and COST was found in this region (see Figs. 3D, 3E, lower half), compared with directly adjacent areas with intact SCP and DCP perfusion (see Fig. 3, upper half). In areas with intact SCP and DCP perfusion, including areas directly adjacent to regions with DCP nonperfusion, 12 MP spots located in these regions of interest showed unaffected retinal sensitivity ranging from 29 to 32 dB, whereas only 2 MP spots revealed mildly affected retinal sensitivity (22 dB and 25 dB; see Fig. 2C, yellow box, Supplementary Fig. S2C; yellow box). Altogether, within the area covered by the central 6 × 6 mm SS-OCTA scan, mean retinal sensitivity in the areas with intact SCP and DCP perfusion was 28.2 ± 1.5 dB compared to 10.8 ± 5.4 dB in areas with DCP nonperfusion (mixed model:

Investigative Ophthalmology & Visual Science

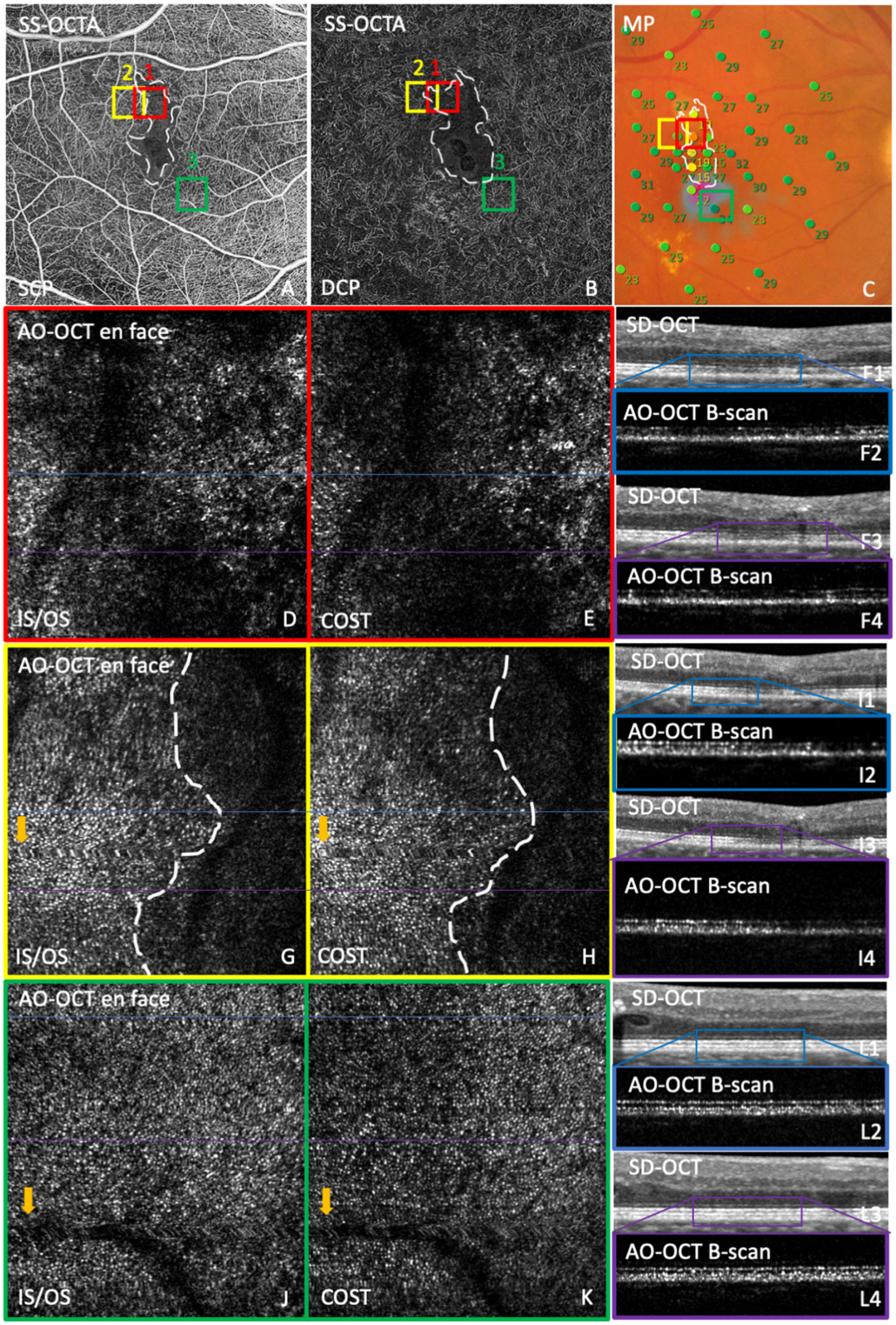

Figure 2. Multimodal imaging of the right eye of a 58-year-old patient with diabetes type II and moderate DR (patient 1). OCTA shows impaired flow (*dark areas*) both at the superficial capillary plexus (SCP) (**A**) and deep capillary plexus (DCP) (**B**) superiorly to the fovea in the area within the *white dotted line* **A** and **B**. In the AO-OCT en face images severe PR signal attenuation at the level of ISOS and COST is seen in the ischemic areas (**D, E; G, H**, right from the *white dotted line*). In areas with intact SCP and DCP perfusion **A** to **C** (left half of the *yellow box* and *green box*) PRs are visualized as densely packed bright white dots **G** and **H** (left from the *white dotted line*; **J, K**) Analogously, the AO-OCT B-scans show hyporeflectivity or total loss of the individual PR signals both at the axial position of ISOS and COST in the ischemic areas (F2, F4; I2, I4, right half). In areas with intact perfusion the PR layer can visualized as two hyper-reflective and clearly separable bands, the upper corresponding to the ISOS, the lower to the COST, with the retinal pigment epithelium visible underneath (I1, I3, left half; L1, L3). In the ischemic area, retinal sensitivity was severely reduced **C** (*red box*; 7 dB), compared to the perfused region just temporal from the ischemic area **C** (*yellow box*; 27 dB) as well as the perfused area without adjacent ischemia **C** (*green box*; 32 dB).

Investigative Ophthalmology & Visual Science

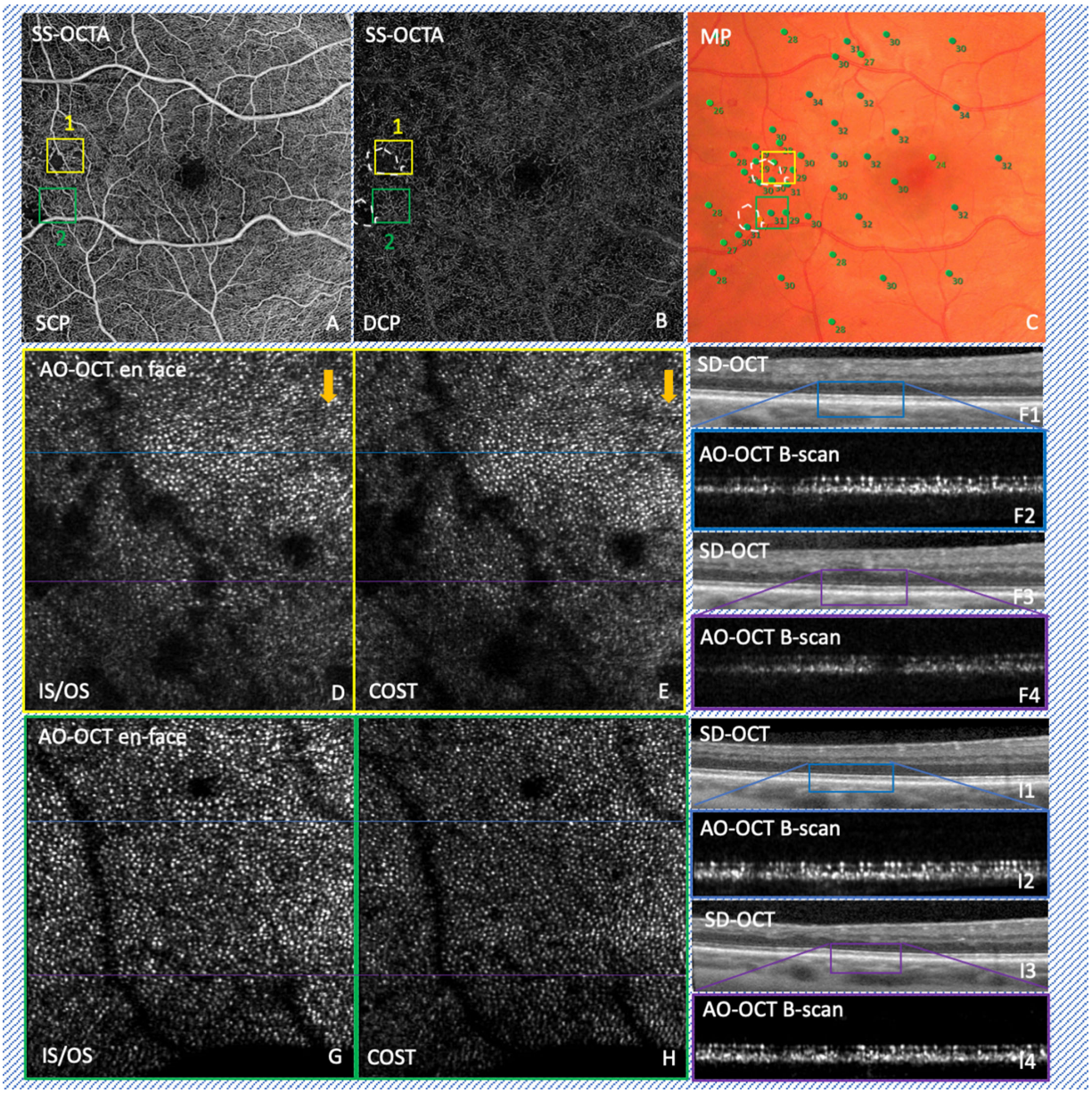

Figure 3. Multimodal imaging of a 34-year-old male patient with diabetes type I and moderate DR (patient 2). Optical coherence tomography angiography (OCTA) shows a small area of superficial capillary plexus (SCP) and deep capillary plexus (DCP) nonperfusion located in the temporal macula (**A, B**; *upper white dotted circle*). AO-OCT enface volumes revealed PR signal attenuation both at the axial position of IS/OS and COST in the area affected by DCP non-perfusion (**D, E**, lower half). In contrast, PR signals were bright a regularly aligned at the axial position of the IS/OS and COST in an area with intact SCP and DCP perfusion, just outside the area of DCP non-perfusion **D** and **E** (upper half) as well as in another spot with intact SCP and DCP perfusion **A** and **C** (*green box* and **G**, **H**). Analogously, the AO-OCT B-scans show hyporeflectivity or loss of PR signals in the area affected by DCP nonperfusion both at the level of IS/OS and COST (F4) compared to areas with intact SCP and DCP perfusion (F2, I2, I4). SD-OCT shows an intact PR layer in the area with intact DCP perfusion (F1, *blue box*). The PR layer seems to be intact, but is not as homogenous in the area affected by DCP nonperfusion (F3, *violet box*) compared to the area with intact DCP perfusion (F1, *blue box*). MP showed unaffected retinal sensitivity in the small area of DCP nonperfusion (27 to 30 dB) **C** (*yellow box*). In another spot with intact SCP and DCP perfusion, retinal sensitivity ranged from 29 dB to 31 dB **C** (*green box*). MP revealed severely reduced retinal sensitivity (7 dB) in an area with SCP and DCP nonperfusion **A** and **C** (within the *lower white dotted circle*). However, this spot was out of range for AO-OCT image acquisition. The tip of the orange arrow points at a small movement artefact **D** and **E**.

estimate 95% confidence interval [CI]; 18.4, 95% CI = 16.6; 20.1, $P < 0.0001$).

For a detailed description of patients 1 and 2, see Figures 2 and 3. Details of patients 3 and 4 are presented in the Supplement Material (see Supplementary Figs. S1, S2).

Discussion

In our study, we analyzed PR signal densities in areas with and without DCP nonperfusion using an AO-OCT prototype and correlated these findings with corresponding retinal sensitivity measurements as assessed by microperimetry.

Investigative Ophthalmology & Visual Science

Table 1. Summary of the Demographic Parameters of the Study Patients

Patient No.	Age	DM Type	DM Duration	HbA1c in %	DR Stage	BCVA	Ocular Pretreatment	No. of Anti-VEGF Injections	Systemic Disease
1	58	II	2 y	7.5	Moderate	20/32	Anti-VEGF	9	Hypertension
2	34	I	22 y	7.3	Moderate	25/20	Non	–	Non
3	38	I	34 y	7.1	Quiescent proliferative	20/20	PRP	–	Non
4	60	II	7 y	7.6	Active proliferative	20/40	Anti-VEGF	5	Hypertension

DM = diabetes mellitus, DR = diabetic retinopathy, BCVA = best-corrected visual acuity, No. = number.

Table 2. Photoreceptor (PR) Signal Density Values for all Spots of all Patients

Patient	Spot no.	Horizontal Foveal ECC.	Vertical Foveal ECC.	Perfusion Status	PR Signal Density IS/OS/mm^2	PR Signal Density ETPR/mm^2
1 (OD)	1	0.6 degrees n	+3.0	SCP− // DCP−	7652	7565
	2	1.6 degrees n	+3.0	SCP+ // DCP−SCP+ // DCP+	593611,377	669211,144
	3	1.6 degrees t	−3.0	SCP+ // DCP+	12,191	11,842
	4	1.6 degrees t	+3.0	SCP− // DCP−SCP+ // DCP+	446610,373	362210,547
2 (OD)	1	8.0 degrees n	+0.5	SCP− // DCP−SCP+ // DCP+	33145274	31075313
	2	8.5 degrees n	+0.5	SCP− // DCP−	2811	2682
	3	8.5 degreesn	−1.8	SCP+ // DCP+	4758	4797
2 (OS)	1	8 degrees t	+0.5	SCP+ // DCP+	4987	4797
	2	8.5 degrees t	−1.8	SCP+ // DCP+	5302	5289
3 (OD)	1	1.8 degrees n	+4.2	SCP− // DCP−	5515	6428
	2	0 degrees	−6.5	SCP+ // DCP+	9423	9139
	3	3.1 degrees t	+4.7	SCP+ // DCP−SCP+ // DCP+	690110,935	668111,660
4 (OD)	1	2.1 degrees n	+3.3	SCP− // DCP−SCP+ // DCP+	904812,853	868913,441
	2	3.3 degrees t	+2.1	SCP+ // DCP+	13,098	12,772
	3	3.6 degrees n	−2.9	SCP+ // DCP+	13,131	12,984
	4	3.6 degrees n	−5.6	SCP+ // DCP+	11,890	14,176

No. = number, ecc. = eccentricity, IS/OS = inner-segment outer-segment, COST = cone outer segment tips, n = nasal, t = temporal, SCP = superficial capillary plexus, DCP = deep capillary plexus.

We found that PR morphology was severely altered in all eight ischemic regions of interest and unremarkable in the vast majority with intact capillary perfusion and mildly affected in a few of them. Further, our results demonstrate a significant reduction of PR signal density both at the axial position of IS/OS and COST by almost 40% in areas affected by DCP nonperfusion compared with areas with intact SCP and DCP perfusion. Further, AO-OCT revealed alterations in the different PR layers both at the axial position of IS/OS and COST, characterized by attenuation or loss of PR reflectivity. In contrast, in areas with intact SCP and DCP, perfusion PRs appeared as bright white, densely packed, and predominantly hyper-reflective dots.

Studies using an AO fundus camera or AO scanning laser ophthalmoscope imaging to investigate differences in PR densities between patients with different stages of DR yielded contradictory results concerning the influence of increasing DR severity on PR signal density.[32–35] In these studies, the presence of DMI was not evaluated. However, the results of our study and previously published work show that the presence of DMI colocalizes with alterations in the PR layer.[14,36,37] As the extent of DMI rises with increasing DR severity, differences in PR signal densities found between different stages of DR may be attributable to the presence of DMI rather than DR.[8] Thus, future studies investigating PR signal densities in diabetic eyes should aim to combine AO-assisted imaging with OCTA to address this question.

Interestingly, despite the advanced stages of DR in our patient cohort (3 eyes with moderate DR and 2 eyes with proliferative DR) retinal function outside the areas affected by DCP nonperfusion was almost unaffected. In contrast, retinal sensitivity in areas affected by DCP nonperfusion was severely reduced. A recently published study on the effect of DCP nonperfusion on PR layer integrity and the corresponding retinal function using OCTA and microperimetry yielded similar results.[15] Hence, it could be hypothesized that DR in the absence of DMI might indeed not have such a deleterious effect on PRs and subsequently on retinal function. This would explain why PR signal density and morphology in areas with intact capillary perfusion in the diabetic eyes analyzed in the current study were comparable to a larger sample of healthy subjects recently examined with the same AO-OCT prototype.[25]

In our study, microperimetry was performed within approximately 5 degrees around the center of the fovea using standardized grids. We found that retinal sensitivity was indeed almost unaffected in areas with intact DCP perfusion throughout the whole area examined (see Figs. 2A–C, 3A–C, Supplementary Figs. S1A–C, Supplementary S2A–C – outside the white dotted circle). Most retinal sensitivity values we obtained were therefore not biased by specific selection of spots. Additional spots were manually placed almost exclusively in and around the ischemic areas. Thus, we were able to gain dense information in the border

regions between ischemic and perfused retina, which also showed that they were unaffected to mildly reduced retinal sensitivity in these areas. What is more, due to the strict inclusion criteria that were needed for the acquisition of the AO-OCT images, our microperimetry data is free from bias attributable to media opacities. They are of course limited by the small number of eyes included in this study, yet this interesting finding could encourage future studies to investigate retinal sensitivity more closely in DR, especially in the border region between intact and impaired capillary perfusion of the retina as well as in areas with sparse capillary perfusion.

Regarding the AO-assisted visualization of PRs, Nesper et al. evaluated the en face cone packing arrangement in patients with diabetes with deep capillary plexus nonperfusion using AO scanning laser ophthalmoscope.[37] The authors found an abnormal arrangement of cones in nonperfused areas in eight diabetic eyes compared with areas with intact perfusion in three diabetic eyes of patients with type I and II diabetes. Increasing irregularities of the PR mosaic correlated significantly with reduced vessel densities in the DCP, as assessed with OCTA.[37] However, neither a quantification of PR signal density nor retinal sensitivity testing was performed in this study. Thus, our study adds important information regarding depth resolved quantification or PR densities both at the axial position of IS/OS and COST combined with functional testing in areas with and without DCP nonperfusion. In a number of diabetic animal models, PR loss was also reported.[38–41] It is unclear if the PR loss we observed in our study eyes is either due to retinal capillary nonperfusion, a response secondary to alterations in the choriocapillaris, the choroid or the retinal pigment epithelium, or caused by neurodegenerative processes directly involving the PRs as the underlying mechanisms are still not fully elucidated. It is known, that apart from the choroidal circulation, the DCP also contributes 10% to 15% to photoreceptor oxygenation, which further highlights the importance of the DCP for photoreceptor functioning and survival.[42] Impaired oxygen delivery to PRs in the presence of a diabetic choroidal or choriocapillaris vasculopathy, as demonstrated in post mortem eyes of patients with diabetes, might increase PR vulnerability, hence leading to loss of PRs and retinal function.[15,43–46] Regarding the role of the choriocapillaris for PR survival, previous clinical studies employing OCTA have demonstrated a colocalization between photoreceptor loss and impaired choriocapillaris perfusion in patients with geographic atrophy or Stargardt disease.[47,48] In diabetic eyes, a general association but not colocalization among an increased extent of choriocapillaris flow deficits, decreased retinal function, and alterations in the PR layer has been demonstrated in the macular region compared to healthy controls.[49,50] However, due to the limitations of currently commercially available OCTA devices a detailed analysis of the choriocapillaris is not yet possible. Because the extent of choriocapillaris flow deficits in healthy individuals reaches up to 40%, a differentiation between physiological flow deficits and those attributable to DR or DMI remains subject to interpretation.[49] In the future, technological improvements of OCTA imaging will give additional insights into the role of the choriocapillaris for the sequence of pathological changes that ultimately lead to PR damage and loss of retinal function in patients with DMI.

PR damage in the course of DMI may also be triggered by retinal Müller cells (MCs), the primary glial cells in the retina, which play a crucial role in maintaining PR metabolism and survival.[51,52] Under physiologic conditions, MCs provide PRs with lactate that serves as an additional source of energy and might contribute to their survival and functioning especially in the presence of compromised capillary perfusion of the retina and choroid as seen in the course of DR.[53] Furthermore, in a transgenic mouse model with inhibited MCs, reduced flash responses in electroretinography, reflecting impaired function of cones, rods, and MCs, were found. Additionally, histological staining revealed patchy loss of photoreceptor outer segments in these mice, whereas a regular staining pattern was found in wild type mice. Further, it was shown that areas of capillary dropout colocalized with loss of photoreceptor outer segments after MC inhibition. These findings highlight the close connection between MC dysfunction, the retinal microcirculation, and photoreceptor survival.[51]

Strengths of this study include the combination of innovative imaging and functional test approaches using an AO-OCT prototype for the three-dimensional visualization of single PRs, OCTA for evaluation of retinal ischemia, as well as fundus-guided microperimetry to assess retinal sensitivity. Limitations include the restriction of analysis to five eyes of four patients with diabetes. However, multimodal imaging and especially the combination of AO-OCT and microperimetry is challenging. The limitations of both technologies lie in the difficulty to acquire information at the very spot of interest, especially when investigating changes on such a small scale as required for this study. Additionally, conditions, such as the presence of diabetic macular edema, hard exudates, hemorrhages, or epi-retinal membranes in the regions of interest, strongly limited the number of patients eligible for this study. Another limitation is the potential presence of other causes of reduced retinal sensitivity due to diabetic neurodegeneration inaccessible with the methodology used in our study.

In conclusion, the data from our study add valuable information to the important relationship between retinal structure and function in DMI by linking retinal capillary dropout at the level of the DCP to PR impairment and reduced retinal sensitivity. Multimodal imaging studies combining AO-assisted visualization of PRs, depth resolved OCTA-guided detection of capillary changes with fundus-guided functional retinal testing will help to better understand the temporal course of DMI in DR. Parameters assessed by advanced retinal imaging and sensitivity test technologies might serve as biomarkers to monitor treatment success in future therapeutic studies that aim to prevent the progression of microcapillary and neurodegenerative changes and associated visual loss in early DR.

Acknowledgments

Financial support from European project FAMOS (FP7 317744).

Disclosure: **F. Datlinger**, None; **L. Wassermann**, None; **A. Reumueller**, None; **D. Hajdu**, None; **I. Steiner,** None; **M. Salas**, None; **W. Drexler**, Meditec (C), Insight (C); **M. Pircher**, Imagine Eyes (F, C); **U. Schmidt-Erfurth**, None; **A. Pollreisz**, None

References

1. Garner A. Histopathology of diabetic retinopathy in man. *Eye*. 1993;7(2):250–253.

2. Engerman RL. Perspectives in diabetes pathogenesis of diabetic retinopathy, https://diabetes.diabetesjournals.org/content/diabetes/38/10/1203.full.pdf.
3. Early Treatment Diabetic Retinopathy Study Research Group. Classification of diabetic retinopathy from fluorescein angiograms: ETDRS report number 11. *Ophthalmology*. 1991;98(5):807–822.
4. Sim DA, Keane PA, Zarranz-Ventura J, et al. The effects of macular ischemia on visual acuity in diabetic retinopathy. *Invest Ophthalmol Vis Sci*. 2013;54(3):2353–2360.
5. Ticho U, Patz A. The role of capillary perfusion in the management of diabetic macular edema. *Am J Ophthalmol*. 1973;76(6):880–886.
6. Bresnick GH, De Venecia G, Myers FL, Harris JA, Davis MD. Retinal ischemia in diabetic retinopathy. *Arch Ophthalmol*. 1975;93(12):1300–1310.
7. Klein R, Klein BE, Moss SE. Visual impairment in diabetes. *Ophthalmology*. 1984;91(1):1–9.
8. Early Treatment Diabetic Retinopathy Study Research Group. Fluorescein angiographic risk factors for progression of diabetic retinopathy: ETDRS report number 13. *Ophthalmology*. 1991;98(5):834–840.
9. Chung EJ, Roh MI, Kwon OW, Koh HJ. Effects of macular ischemia on the outcome of intravitreal bevacizumab therapy for diabetic macular edema. *Retina*. 2008;28(7):957–963.
10. Sim DA, Keane PA, Zarranz-Ventura J, et al. Predictive factors for the progression of diabetic macular ischemia. *Am J Ophthalmol*. 2013;156(4):684–692.e1.
11. Douvali M, Chatziralli IP, Theodossiadis PG, Chatzistefanou KI, Giannakaki E, Rouvas AA. Effect of macular ischemia on intravitreal ranibizumab treatment for diabetic macular edema. *Ophthalmologica*. 2014;232(3):136–143.
12. Bresnick GH, Condit R, Syrjala S, Palta M, Groo A, Korth K. Abnormalities of the foveal avascular zone in diabetic retinopathy. *Arch Ophthalmol*. 1984;102(9):1286–1293.
13. Cheung CMG, Wong TY. Clinical use of optical coherence tomography angiography in diabetic retinopathy treatment ready for showtime? *JAMA Ophthalmol*. 2018;136(7):729–730.
14. Scarinci F, Nesper PL, Fawzi AA. Deep retinal capillary nonperfusion is associated with photoreceptor disruption in diabetic macular ischemia. *Am J Ophthalmol*. 2016;168:129–138.
15. Scarinci F, Varano M, Parravano M. Retinal sensitivity loss correlates with deep capillary plexus impairment in diabetic macular ischemia. *J Ophthalmol*. 2019;2019:7589841.
16. Rohrschneider K, Bültmann S, Springer C. Use of fundus perimetry (microperimetry) to quantify macular sensitivity. *Prog Retin Eye Res*. 2008;27(5):536–548.
17. Hanout M, Horan N, Do D V. Introduction to microperimetry and its use in analysis of geographic atrophy in age-related macular degeneration. *Curr Opin Ophthalmol*. 2015;26(3):149–156.
18. Liang J, Williams DR, Miller DT. Supernormal vision and high-resolution retinal imaging through adaptive optics. *J Opt Soc Am A Opt Image Sci Vis*. 1997;14(11):2884.
19. Roorda A, Williams DR. The arrangement of the three cone classes in the living human eye. *Nature*. 1999;397(6719):520–522.
20. Roorda A, Romero-Borja F, Donnelly WJ, III, Queener H, Hebert TJ, Campbell MCW. Adaptive optics scanning laser ophthalmoscopy. *Opt Express*. 2002;10(9):405.
21. Hermann B, Fernández EJ, Unterhuber A, et al. Adaptive-optics ultrahigh-resolution optical coherence tomography. *Opt Lett*. 2004;29(18):2142.
22. Pircher M, Zawadzki RJ. Review of adaptive optics OCT (AO-OCT): principles and applications for retinal imaging [Invited]. *Biomed Opt Express*. 2017;8(5):2536.
23. Reumueller A, Schmidt-Erfurth U, Salas M, et al. Three-dimensional adaptive optics–assisted visualization of photoreceptors in healthy and pathologically aged eyes. *Invest Opthalmol Vis Sci*. 2019;60(4):1144.
24. Curcio CA, Sloan KR, Kalina RE, Hendrickson AE. Human photoreceptor topography. *J Comp Neurol*. 1990;292(4):497–523.
25. Reumueller A, Wassermann L, Salas M, et al. Three-dimensional assessment of para- and perifoveal photoreceptor densities and the impact of meridians and age in healthy eyes with adaptive-optics optical coherence tomography (AO-OCT). *Opt Express*. 2020;28(24):36723.
26. Chylack LT. The Lens Opacities Classification System III. *Arch Ophthalmol*. 1993;111(6):831.
27. Hafner J, Salas M, Scholda C, et al. Dynamic changes of retinal microaneurysms in diabetes imaged with in vivo adaptive optics optical coherence tomography. *Invest Opthalmol Vis Sci*. 2018;59(15):5932.
28. Karst SG, Salas M, Hafner J, et al. Three-dimensional analysis of retinal microaneurysms with adaptive optics optical coherence tomography. *Retina*. 2019;39(3):465–472.
29. Reumueller A, Wassermann L, Salas M, et al. Morphologic and functional assessment of photoreceptors after macula-off retinal detachment with adaptive-optics OCT and microperimetry. *Am J Ophthalmol*. 2020;214:72–85.
30. Salas M, Drexler W, Levecq X, et al. Multi-modal adaptive optics system including fundus photography and optical coherence tomography for the clinical setting. *Biomed Opt Express*. 2016;7(5):1783–1796.
31. Salas M, Augustin M, Ginner L, et al. Visualization of microcapillaries using optical coherence tomography angiography with and without adaptive optics. *Biomed Opt Express*. 2017;8(1):207–222.
32. Lombardo M, Parravano M, Lombardo G, et al. Adaptive optics imaging of parafoveal cones in type 1 diabetes. *Retina*. 2014;34(3):546–557.
33. Tan W, Wright T, Rajendran D, et al. Cone–photoreceptor density in adolescents with Type 1 Diabetes. *Invest Opthalmol Vis Sci*. 2015;56(11):6339.
34. Soliman MK, Sadiq MA, Agarwal A, et al. High-resolution imaging of parafoveal cones in different stages of diabetic retinopathy using adaptive optics fundus camera. *PLoS One*. 2016;11(4):e0152788.
35. Lammer J, Prager SG, Cheney MC, et al. Cone photoreceptor irregularity on adaptive optics scanning laser ophthalmoscopy correlates with severity of diabetic retinopathy and macular edema. *Invest Ophthalmol Vis Sci*. 2016;57(15):6624–6632.
36. Scarinci F, Jampol LM, Linsenmeier RA, Fawzi AA. Association of diabetic macular nonperfusion with outer retinal disruption on optical coherence tomography. *JAMA Ophthalmol*. 2015;133(9):1036.
37. Nesper PL, Scarinci F, Fawzi AA. Adaptive optics reveals photoreceptor abnormalities in diabetic macular ischemia. *PLoS One*. 2017;12(1):e0169926.
38. Miyamura N, Amemiya T. Lens and retinal changes in the WBN/Kob rat (spontaneously diabetic strain). *Ophthalmic Res*. 1998;30(4):221–232.
39. Park S-H, Park J-W, Park S-J, et al. Apoptotic death of photoreceptors in the streptozotocin-induced diabetic rat retina. *Diabetologia*. 2003;46(9):1260–1268.
40. Hammoum I, Mbarek S, Dellaa A, et al. Study of retinal alterations in a high fat diet-induced type ii diabetes rodent: Meriones shawi. *Acta Histochem*. 2017;119(1):1–9.

Investigative Ophthalmology & Visual Science

41. Hammoum I, Benlarbi M, Dellaa A, et al. Study of retinal neurodegeneration and maculopathy in diabetic Meriones shawi : A particular animal model with human-like macula. *J Comp Neurol*. 2017;525(13):2890–2914.
42. Lnur Birol G, Wang S, Budzynski E, Wangsa-Wirawan ND, Linsenmeier RA. Oxygen distribution and consumption in the macaque retina. *Am J Physiol Hear Circ Physiol*. 2007;293:1696–1704.
43. Cao J, McLeod DS, Merges CA, Lutty GA. *Arch Ophthalmol*. 1998;116(5):589–597.
44. Hidayat AA, Fine BS. Diabetic Choroidopathy: Light and electron microscopic observations of seven cases. *Ophthalmology*. 1985;92(4):512–522.
45. Fryczkowski AW, Hodes BL, Walker J. Diabetic choroidal and iris vasculature scanning electron microscopy findings. *Int Ophthalmol*. 1989;13(4):269–279.
46. Cao J, McLeod DS, Merges CA, Lutty GA. Choriocapillaris degeneration and related pathologic changes in human diabetic eyes. *Arch Ophthalmol*. 1998;116(5):589–597.
47. Sacconi R, Corbelli E, Borrelli E, et al. Choriocapillaris flow impairment could predict the enlargement of geographic atrophy lesion. *Br J Ophthalmol*. 2021;105(1):97–102.
48. Alabduljalil T, Patel RC, Alqahtani AA, et al. Correlation of outer retinal degeneration and choriocapillaris loss in Stargardt disease using en face optical coherence tomography and optical coherence tomography angiography. *Am J Ophthalmol*. 2019;202:79–90.
49. Ro-Mase T, Ishiko S, Omae T, Ishibazawa A, Shimouchi A, Yoshida A. Association between alterations of the choriocapillaris microcirculation and visual function and cone photoreceptors in patients with diabetes. *Invest Ophthalmol Vis Sci*. 2020;61(6):1.
50. Borrelli E, Palmieri M, Viggiano P, Ferro G, Mastropasqua R. Photoreceptor damage in diabetic choroidopathy. *Retina*. 2020;40(6):1062–1069.
51. Shen W, Fruttiger M, Zhu L, et al. Conditional müller cell ablation causes independent neuronal and vascular pathologies in a novel transgenic model. *J Neurosci*. 2012;32(45):15715–15727.
52. Coughlin BA, Feenstra DJ, Mohr S. Müller cells and diabetic retinopathy. *Vision Res*. 2017;139:93–100.
53. Poitry-Yamate CL, Poitry S, Tsacopoulos M. Lactate released by Muller glial cells is metabolized by photoreceptors from mammalian retina. *J Neurosci*. 1995;15(7 II):5179–5191.

Investigative Ophthalmology & Visual Science